THE EFFECT OF COOLING ON MECHANICAL AND THERMAL STRESSES IN VASCULAR STRUCTURES

E. Cetkin[1,*]

ABSTRACT

Here, we show how the vascular channel configuration and its shape affect the mechanical strength which is simultaneously subjected to heating and mechanical load. The material properties were defined as functions of temperature. The effect of channel cross-section on the coolant mass flow rate, peak temperature and peak stresses are documented. The results show that the resistances to flow of stresses and fluid is minimum with the circular channels while the resistance to the heat flow is the smallest with semi-circular channels. In addition, morphing the vascular design provides almost the smallest resistance to the heat flow with circular channels (0.3% difference in the peak temperature). This shows that even the convective resistances are the smallest with circular-cross section, overall thermal resistance is smaller in semi-circular design for the fixed fluid volume. The peak stress is smaller with hybrid design than the parallel designs for the entire pressure drop range. In addition, the effects of mechanical load, heating rate and reference temperature on the stress distribution are also documented. Furthermore, the thermal and mechanical stresses are also documented separately, and then compared with the coupled solution cases. The chief result of this paper is that for a coupled system minimizing only one of the resistance terms is not sufficient, all the resistances considered simultaneously in order to uncover the best performing design. In coupled solutions, we documented the simulation results with temperature dependent material properties and the resistances to the heat and fluid flow is affected by the mechanical deformations. In addition, the results show that the designs should be free to vary, the unexpected designs can be the best performing designs for the given parameters and constraints. Therefore, the design parameters based on the experience does not always yield the best performing designs as the objectives and constraints vary.

Keywords: Vascular, Cooling, Thermal Expansion, Smart Features

INTRODUCTION

Advanced technologies require great volumetric cooling capacities due to the trend of miniaturization [1-2]. Heat transfer surface area is limited in miniature designs. Therefore, the current literature focuses on heat transfer enhancement methods with nano-fluids and phase change [3-9]. These methods are essential in order to increase the heat transfer rate. However, heat load can be deterministic and random [10]. Future technologies require miniature structures which are capable of cooling itself under deterministic and random cooling loads. This requirement can be satisfied with self-cooling structures [10-17]. However, they should also be capable of supporting themselves under the applied mechanical load and/or their weight.

Materials with smart capabilities were suggested by White et al. in 2001 [18]. They mimicked the self-healing mechanism of animals by documenting a polymer composite structure which seals itself when crack occurs (similar to clot occurrence at the wound in order to seal it). However, their autonomic healing concept is a one time solution because healing agents were placed in spheres which can be used once. Later, Hamilton et al. claimed that vascular structures enables it to heal itself countless time similar to the circulatory systems of warm blooded animals [19]. Bejan et al. showed that vascularized structures can also be used to cool a domain on which heat load applied [20]. Wang et al. uncovered how the mechanical strength of a vascular domain varies as the channel design and volume fraction vary [21]. Later, Cetkin et al. showed how the mechanical strength and cooling performance is affected by the volume fraction and by the shape of the channel configurations [14]. Cetkin et al. uncovered that vascularization provides required cooling both deterministic and random cooling requirements [10]. Cetkin uncovered the effect of straight and wavy vascular channels on the cooling performance [22]. In addition, the current literature also shows how vascularized structures increase the mechanical strength of a heated domain with applied heating and mechanical load with the effect of thermal expansion [23-24]. The current literature documents the simulation results with constant material properties and the effect of deformation is not

effecting the resistances to the heat and fluid flow. In addition, the current literature lacks of documenting the effect of cross-section on the mechanical and thermal performance with the effect of thermal stresses.

This paper uncovers how the novel hybrid and parallel vascular structures discussed in the literature [15] performs under applied mechanical load and thermal expansion. The effect of cross-section of the vascular channels on the thermal performance and mechanical strength is also uncovered simultaneously with the consideration of thermal stresses. The material properties in the simulations are functions of temperature. In addition, the solution includes the effect of temperature distribution on the material properties and thermal stresses and the effect of deformation on the heat and fluid flow resistances.

MODEL

Consider the vascular structure with embedded semi-circular cooling channels which is shown in Figure 1a. The plate is uniformly heated and loaded on x-z surface along the y direction. The periphery boundaries of the plate are no displacement boundaries, and all the surfaces except the fluid flow inlet ($T = T_{in}$) boundary is thermal symmetry boundaries ($\partial T / \partial n = 0$). The fluid flow is driven by the pressure difference between the inlet and outlet boundaries ($\Delta P = P_{in} - P_{out}$). The boundary conditions can also be seen on Figure 1a. In addition, the fluid and solid domain volume are fixed, so their ratio (V_f). The material properties of the coolant and solid are given in Table 1.

Table 1. Thermo-physical properties at atmospheric pressure for water and Aluminium 3003 [24]

	Water	Aluminium3003
ρ	998.2	2729.2
k	$-0.869 + 8.949 \times 10^{-3} T - 1.584 \times 10^{-5} T^2 + 7.975 \times 10^{-9} T^3$	$75.779 + 1.279T - 8.263 \times 10^{-3} T^2 + 2.487 \times 10^{-5} T^3 - 2.815 \times 10^{-8} T^4$
c_p	$12010.147 - 80.407T + 0.309T^2 - 5.381 \times 10^{-4} T^3 + 3.625 \times 10^{-7} T^4$	$-264.783 + 9.293T - 1.210 \times 10^{-2} T^2 - 6.741 \times 10^{-5} T^3 + 1.655 \times 10^{-7} T^4$
μ	$1.379 - 2.122 \times 10^{-2} T + 1.360 \times 10^{-4} T^2 - 4.645 \times 10^{-7} T^3 + 8.904 \times 10^{-10} T^4 - 9.079 \times 10^{-13} T^5 + 3.84610^{-16} T^6$	-
α	-	$1.967 \times 10^{-5} + 1.207 \times 10^{-8} T - 3.632 \times 10^{-12} T^2$
γ	-	$0.324 + 3.754 \times 10^{-6} T + 2.214 \times 10^{-7} T^2 - 6.565 \times 10^{-10} T^3 + 4.213 \times 10^{-13} T^4 + 3.171 \times 10^{-16} T^5$
E	-	$7.770 \times 10^{10} + 203.649 \times 10^4 T - 189.161 \times 10^3 T^2 + 425.293T^3 - 0.355T^4$

The fluid flow is governed by the conservation of mass and momentum equations for incompressible and steady flow;

$$\frac{\partial u}{\partial x} + \frac{\partial v}{\partial y} + \frac{\partial w}{\partial z} = 0 \tag{1}$$

$$u\frac{\partial u}{\partial x} + v\frac{\partial u}{\partial y} + w\frac{\partial u}{\partial z} = -\frac{1}{\rho}\frac{\partial P}{\partial x} + \nu\nabla^2 u \tag{2}$$

$$u\frac{\partial v}{\partial x} + v\frac{\partial v}{\partial y} + w\frac{\partial v}{\partial z} = -\frac{1}{\rho}\frac{\partial P}{\partial y} + \nu\nabla^2 v \tag{3}$$

$$\text{u}\frac{\partial \text{w}}{\partial \text{x}} + \text{v}\frac{\partial \text{w}}{\partial \text{y}} + \text{w}\frac{\partial \text{w}}{\partial \text{z}} = -\frac{1}{\rho}\frac{\partial \text{P}}{\partial \text{z}} + \text{v}\nabla^2 \text{w} \tag{4}$$

where $\nabla^2 = \partial^2/\partial^2\text{x} + \partial^2/\partial^2\text{y} + \partial^2/\partial^2\text{z}$. x, y and z are the spatial coordinates, and u, v and w are the velocity components corresponding to these coordinates, respectively. In addition, P, v and ρ are the pressure, kinematic viscosity and fluid density. The coolant fluid is single phase.

The temperature distribution inside the fluid domain is governed by the energy equation

$$\rho c_p \left(u\frac{dT}{dx} + v\frac{dT}{dy} + w\frac{dT}{dz} \right) = \frac{\partial}{\partial x}\left(k_f \frac{\partial T}{\partial x} \right) + \frac{\partial}{\partial y}\left(k_f \frac{\partial T}{\partial y} \right) + \frac{\partial}{\partial z}\left(k_f \frac{\partial T}{\partial z} \right) \tag{5}$$

where c_p is the specific heat at constant pressure of the fluid, T is temperature, and k_f is the thermal conductivity of the fluid. The temperature distribution inside the solid domain is governed by $\nabla^2 T = 0$. The continuity of heat flux between the solid and fluid interfaces is

$$k_s \frac{\partial T}{\partial n} = k_f \frac{\partial T}{\partial n} \tag{6}$$

where n is the normal vector to the interface.

The elastic deformations on the vascularized structure are small when compared with the length scale of the structure. In addition, there is no volume forces (the effect of the plate weight is neglected because it is so small in comparison with the effects of the applied mechanical load and thermal stresses). With these simplifications in mind, the conservation of the momentum for the solid domain and generalized Hooke's law for heated and mechanically loaded vascular plate become

$$\frac{\partial \sigma_{xx}}{\partial x} + \frac{\partial \tau_{yx}}{\partial y} + \frac{\partial \tau_{zx}}{\partial z} = 0 \tag{7}$$

$$\frac{\partial \tau_{xy}}{\partial x} + \frac{\partial \sigma_{yy}}{\partial y} + \frac{\partial \tau_{zy}}{\partial z} = 0 \tag{8}$$

$$\frac{\partial \tau_{xz}}{\partial x} + \frac{\partial \tau_{yz}}{\partial y} + \frac{\partial \sigma_{zz}}{\partial z} = 0 \tag{9}$$

$$\begin{bmatrix} \sigma_{xx} \\ \sigma_{yy} \\ \sigma_{zz} \\ \tau_{yz} \\ \tau_{zx} \\ \tau_{xy} \end{bmatrix} = \frac{E}{(1+\gamma)(1-2\gamma)} \begin{bmatrix} 1-\gamma & \gamma & \gamma & 0 & 0 & 0 \\ \gamma & 1-\gamma & \gamma & 0 & 0 & 0 \\ \gamma & \gamma & 1-\gamma & 0 & 0 & 0 \\ 0 & 0 & 0 & (1-2\gamma)/2 & 0 & 0 \\ 0 & 0 & 0 & 0 & (1-2\gamma)/2 & 0 \\ 0 & 0 & 0 & 0 & 0 & (1-2\gamma)/2 \end{bmatrix} \begin{bmatrix} \varepsilon_{xx} \\ \varepsilon_{yy} \\ \varepsilon_{zz} \\ \varphi_{yz} \\ \varphi_{zx} \\ \varphi_{xy} \end{bmatrix} \tag{10}$$

$$\begin{bmatrix} \varepsilon_{xx} \\ \varepsilon_{yy} \\ \varepsilon_{zz} \\ \varphi_{yz} \\ \varphi_{zx} \\ \varphi_{xy} \end{bmatrix} = \begin{bmatrix} \varepsilon_{m,xx} \\ \varepsilon_{m,yy} \\ \varepsilon_{m,zz} \\ \varphi_{m,yz} \\ \varphi_{m,zx} \\ \varphi_{m,xy} \end{bmatrix} - (T - T_{ref}) \begin{bmatrix} \alpha \\ \alpha \\ \alpha \\ 0 \\ 0 \\ 0 \end{bmatrix} \tag{11}$$

where γ, α and E are the Poisson ratio, the thermal expansion coefficient and the elasticity modulus, respectively. In addition, the strain displacement relations for small deformations are

$$\varepsilon_{m,xx} = \frac{\partial r_x}{\partial x} \qquad \varepsilon_{m,yy} = \frac{\partial r_y}{\partial y} \qquad \varepsilon_{m,zz} = \frac{\partial r_z}{\partial z} \tag{12}$$

$$\varphi_{m,xy} = \frac{\partial r_x}{\partial y} + \frac{\partial r_y}{\partial x} \qquad \varphi_{m,yz} = \frac{\partial r_z}{\partial y} + \frac{\partial r_y}{\partial z} \qquad \varphi_{m,zx} = \frac{\partial r_z}{\partial x} + \frac{\partial r_x}{\partial z} \qquad (13)$$

where r_x, r_y and r_z are the displacements along the directions of x, y and z, respectively.

NUMERICAL METHOD

Consider the plate with embedded semi-circular channels in parallel configuration as shown in Figures 1a and b. The plate is square with length scale of 120 mm and with thickness of 5 mm. Figure 1b shows three-dimensional sketch of the vascularized plate with parallel configuration. Figure 1a also shows the dimensions in between centre planes of vascular channels and the corner of the plate such as 3 and 10 mm. The numbers without any units have the unit of mm. Figures 1a and 1c show the views from the side and the top where the directions can be seen from the Figure 1a. The coolant fluid is distributed to ten vascular channels of diameter $d_1 = 2.589 \times 10^{-3}$ m through a main distributing channel of diameter $d_0 = 4.674 \times 10^{-3}$ m as shown in Figure 1a. Then, the coolant fluid is collected via a main collecting channel of diameter d. The volume of the coolant fluid is fixed at $V_f = 4 \times 10^{-6}$ m³. Figure 1c shows the schematic of the hybrid design with the same length scales (120 mm and the thickness of 5 mm) and volume fraction ($V_f = 4 \times 10^{-6}$ m³) of the Figure 1a. Therefore, the diameters of the vascular channels in Figure 1c becomes; $d_0 = 3.339 \times 10^{-3}$ m, $d_1 = 2.229 \times 10^{-3}$ m, $d_2 = 1.769 \times 10^{-3}$ m and $d_3 = 1.404 \times 10^{-3}$ m. Figure 1d shows the three-dimensional sketch of the vascularized plate with hybrid channels. The coolant flows in between the inlet and outlet boundaries due to the imposed pressure difference, ΔP, which varies in between 30 Pa to 3 kPa. The plate was loaded mechanically and heated simultaneously on the x-y plane of the plate in the direction of z, Fig 1. Heating rate (q") and uniform mechanical load (P_{load}) vary in between 2 kW/m²–10 kW/m² and 10^5 Pa–10^6 Pa, respectively. The outer surfaces of the plate are symmetry boundaries (except the surface on which heating and mechanical load are applied). In addition, the corners of the plate are no displacement boundaries, and therefore the plate is free to be deformed along the z direction.
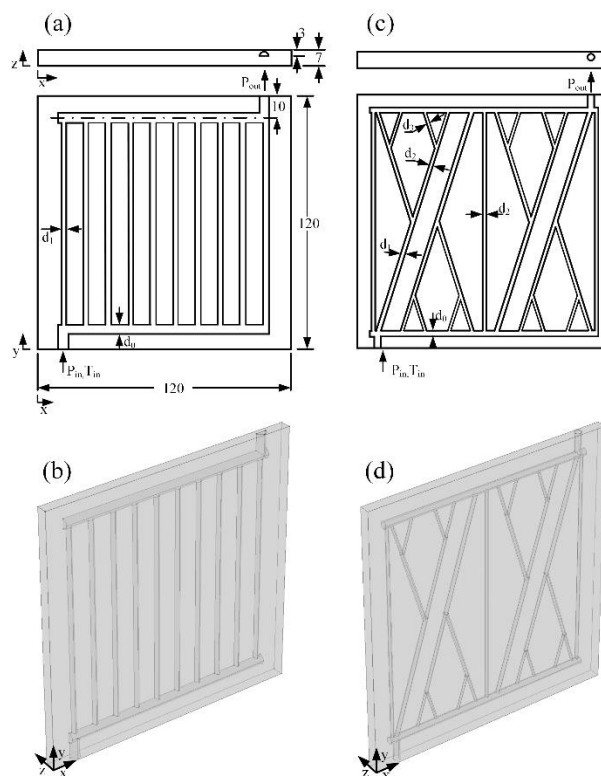

Figure 1. The plate with embedded semi-circular parallel cooling channels; (a) two-dimensional sketch with dimensions and (b) three-dimensional sketch, hybrid cooling channel configuration; (c) two-dimensional sketch with dimensions and (d) three-dimensional sketch [15]

The governing Equations 1 – 10 were solved numerically by a finite element software [25]. Non-uniform mesh with boundary layer meshes near the boundaries were used. The mesh size was decreased until the solution is free of mesh dependency as can be seen from Figure 2a. Figure 2a shows that the effect of mesh size decreases to 0.7% as the number of mesh elements increases from 270638 to 626079. The residual was imposed as 10^{-4} in simulations. In addition, quadratic shape functions were used in discretization.
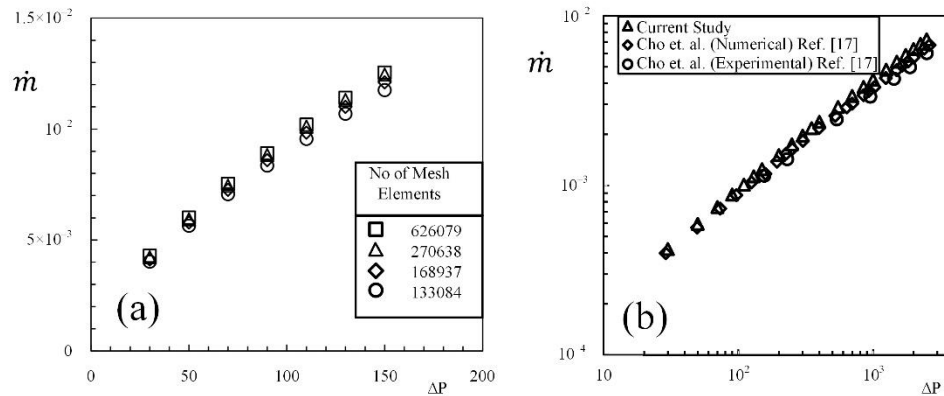

Figure 2. (a)Mesh independency test, (b) Validation of current numerical method with the results [17]

Furthermore, the current results were validated with the numerical and experimental studies of Ref. [17]. Figure 2b shows the current study agrees well with the literature. In addition, the peak temperature documented in this paper agrees well (2% error) with the results documented in Table 3 of Ref. [17]. Therefore, we conclude that the results of the current study are mesh independent and accurate.

PARALLEL CHANNEL DESIGN

Consider that the cross-section of the vascular channels are circular unlike as shown is Fig. 1, which is semi-circular. The circular channels provide smaller fluid flow resistances than semi-circular channels because the hydraulic diameter of the semi-circular channels is less than the diameter of the circular channel for the same volume. Figure 3a show how the pressure drop in between the inlet and outlet boundaries of the coolant affects the mass flow rate for circular and semi-circular parallel designs. The mass flow rate is greater with circular channels in comparison with the semi-circular channels, but the difference increases as the order of the pressure drop increases from 30 to 2000Pa. Changing the channels cross-section from semi-circular to circular increases the mass flow rate % 40 and % 62 for 30 Pa and 2000 Pa, respectively.

Figure 3b shows how the peak temperature in the vascular structure is affected by the pressure drop and channel cross-section. As pressure drop increases, the peak temperature decreases for both circular and semi-circular channels and reaches to an asymptote limit. However, unlike the expectations, the peak temperature with circular channel configurations is greater than the channels with semi-circular cross-sections. The peak temperature is around 350 and 330 K for circular and semi-circular channels when the pressure drop is 30 Pa. As the pressure drop becomes 3000 Pa, the peak temperature becomes 300 and 298 K for circular and semi-circular channels. In addition, increasing the pressure drop after 1000 Pa does not decrease the peak temperature more than 2%. Furthermore, the results of Figures 3a and 3b are in accord with the results of Ref. [15]. This shows the deformations (exists in this study which is not included in Ref. [15]) have negligibly small effect on the resistances to the heat and fluid flow.

Figure 3c shows how the pressure drop and channel cross-section affect the maximum von Mises stress in the solid domain. The peak stress decreases as the pressure difference which drives the coolant flow increases from 30 Pa to 100 Pa, and then it increases as the pressure difference increases with radial semi-circular channels. The peak stress decreases as the pressure difference increases with the radial circular channels. However, the peak stress in circular channel configuration is greater than in semi-circular channels when the pressure difference is less than 600 Pa. After 600 Pa, the peak stress becomes smaller with circular channels in comparison to the semi-circular channels.
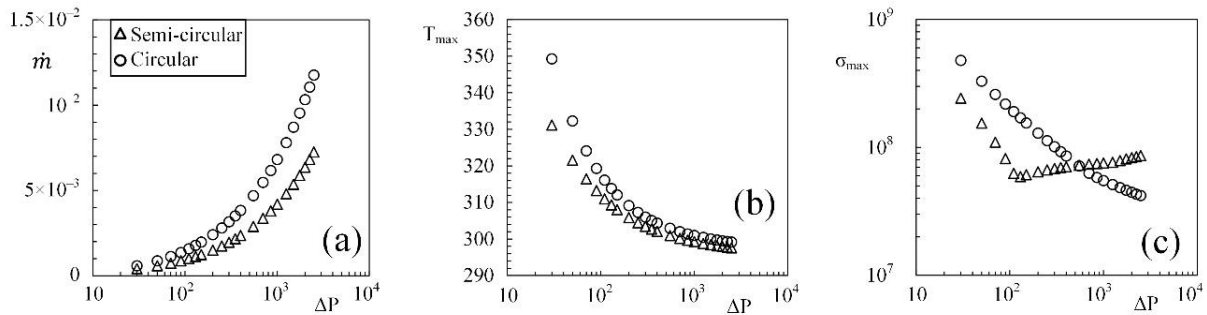
Figure 3. The effect of pressure drop on (a) coolant mass flow rate, (b) maximum temperature and (c) peak stress for circular and semi-circular parallel channel configurations.

The reason of this tendency can be understood better with the results of Figure 3b. Figure 3b shows that as the pressure difference increases the circular and semi-circular channels provide the almost the same peak temperature. This can be considered as eliminating the difference of the stress terms related with the thermal expansion in both designs. The dominating mechanism becomes the mechanical loading. Therefore, the effect of the channel cross-section and its location becomes important which provides smaller peak stress to the circular channels in comparison to the semi-circular ones as the pressure difference increases after 600 Pa. These tendency also explains why the semi-circular parallel channel design corresponds to almost an L shaped curve for maximum von Mises stress. This result suggests the stress field is dominated by the thermal expansion until 100 Pa and then it is dominated by the stress due to the mechanical load. This is more dominant in the semi-circular parallel channels because they have greater diameter than the hybrid design due to the fixed fluid volume constraint. This difference in the diameter both affects the heat transfer surface area and the strength of the plate.

In summary, both circular and semi-circular channel cross-sections have advantages. Circular cross-section provides smaller fluid flow resistance in comparison to semi-circular channels. However, semi-circular channels provide better cooling performance when the heating load is applied only from one surface, i.e. if there were heat generation in the domain then the overall thermal resistance would be smaller in circular channels than in semi-circular ones. The heat transfer surface area which is closest to the surface on which heating applied is bigger in semi-circular channels than in circular ones for the fixed fluid domain volume. Therefore, the semi-circular channels provide smaller peak temperature (especially when the pressure drop is less than 100 Pa for the given design) than the circular channels. In addition, the peak stress is also smaller in semi-circular channels when the pressure difference is less than 100 Pa. Therefore, the semi-circular channels are more favourable when the pressure drop is small, and the circular channels becomes a better option as the pressure drop increases. This should be decided on what are limitations on peak temperature and mass flow rate. Moreover, the results show that the relation in between the thermal stresses and stresses due to the mechanical load should be uncovered in order to understand the physics behind the Figure. 3c. Therefore, the rate of the mechanical and thermal stresses in the overall stress will be uncovered in the next section.

HYBRID DESIGN

Next, consider the hybrid design of tree-shaped and parallel configurations with circular cooling channels as shown in Figure 1c. Parallel cooling channels are placed in between the tree-shaped channels because of the hot spot occurrence in between the channels which was discussed in Ref. [15].

Figure 4 shows how the mechanical loading rate affects the peak stress relative to the maximum temperature for circular hybrid and semi-circular parallel configurations. The pressure difference decreases as the maximum temperature increases. In addition, Figures 4a and b show that the effect of the mechanical load diminishes in the overall peak stress term when the peak temperature is around 330 K and the uniform mechanical load is less than 5×10^5. The peak stress decreases as the mechanical load decreases as expected. However, the tendency of the peak stress relative to the maximum temperature curves vary. Figures 4a and b show that there is a maximum temperature corresponding to the minimum peak temperature for each curve. This peak temperature is close to the reference temperature which is used for thermal stress calculations as shown in Eq. (10). However, it also varies as the design and mechanical load vary. Figures 4a and b show that this temperature is slightly greater in hybrid design (in between 310–320 K) than in parallel design (in between 300–310 K). These results show that

until a limit value increase in the excess temperature actually decreases the peak stress. The reason of this tendency could be better understood with the comparison of the coupled solution results (i.e., mechanical loading is coupled with the thermal expansion) with the segregated solution results (i.e., pure mechanical loading and pure thermal expansion effect).
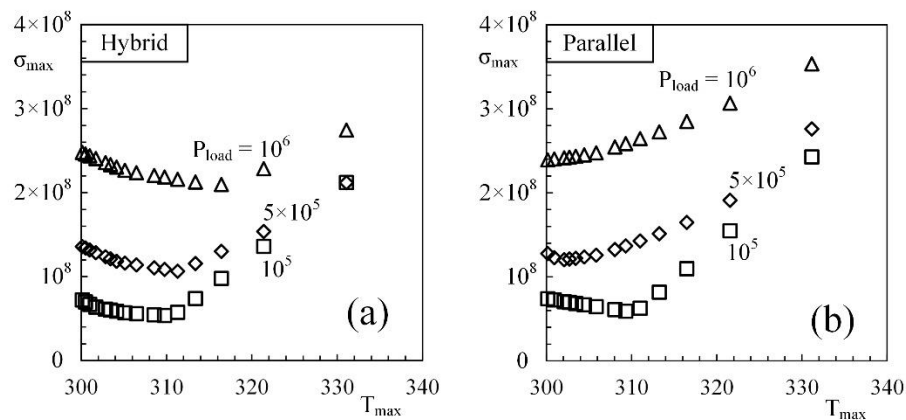

Figure 4. The effect of the maximum temperature on the peak stress with (a) circular hybrid and (b) semi-circular parallel configurations

Figure 5 shows how the peak stress varies relative to the maximum temperature when the effects of mechanical loading and thermal expansion considered both solely and coupled for circular hybrid and semi-circular parallel channels, respectively. Pure mechanical loading results are represented with straight line, sole thermal stresses results are represented with circles and the coupled simulations are represented with squares. Figure 5a, b and c show that the maximum von Mises stress is the greatest in sole mechanical loading case for hybrid design in the entire mechanical loading range, i.e. from 10^5 to 10^6 Pa. This result shows that the effect of thermal expansion actually decreases the maximum stress. The reason is that the thermal expansion occurs in the horizontal direction whereas the mechanical load is applied in the vertical direction. Therefore thermal expansion supports the vascular structure and decreases the displacement along the direction of applied mechanical load. This decreases the effect of mechanical loading in the coupled peak stress results. Figure 5a shows that difference between the sole thermal expansion and coupled simulations is less than 5% when the applied mechanical load is 10^5 Pa. The difference in between the sole thermal stresses and coupled simulations increases as the mechanical load increase, it increases up to 50% and 70% for Figures 5b and c, respectively.

Figures 5d, e, and f show how the peak stress varies relative to the maximum temperature in parallel semi-circular channel configuration for pure thermal stresses, pure mechanical stresses and the coupled stresses for the mechanical loads of 10^5, 5×10^5 and 10^6, respectively. Unlike in Figures. 5a, b and c, the order of the pure thermal stresses is greater than sole mechanical stresses. However, the tendencies of the sole thermal stresses and coupled stresses is similar to their equivalents in Figures. 5a, b and c. The difference between the sole thermal stresses and coupled stresses increases as the mechanical loading increases. In addition, Figure 5 shows that the thermal stresses becomes the minimum at 310 K which is a little bit greater than the reference temperature (303 K). In addition, the Figures 5d, e and f explains the L shaped behaviour of Figure 3c. This L shaped curve of Figure 3c is due to the effect of thermal stresses and its effect diminishes as the stresses due to mechanical load becomes the dominant one in the stress distribution. Overall, Figure 5 shows that the parameters and design corresponding to the minimum peak stress do not correspond to the minimum peak temperature with uniform temperature distribution. Therefore, if the design objective is the minimization of the stresses then the design should be reconsidered, i.e. the design corresponding to the minimum peak temperature should not be used.
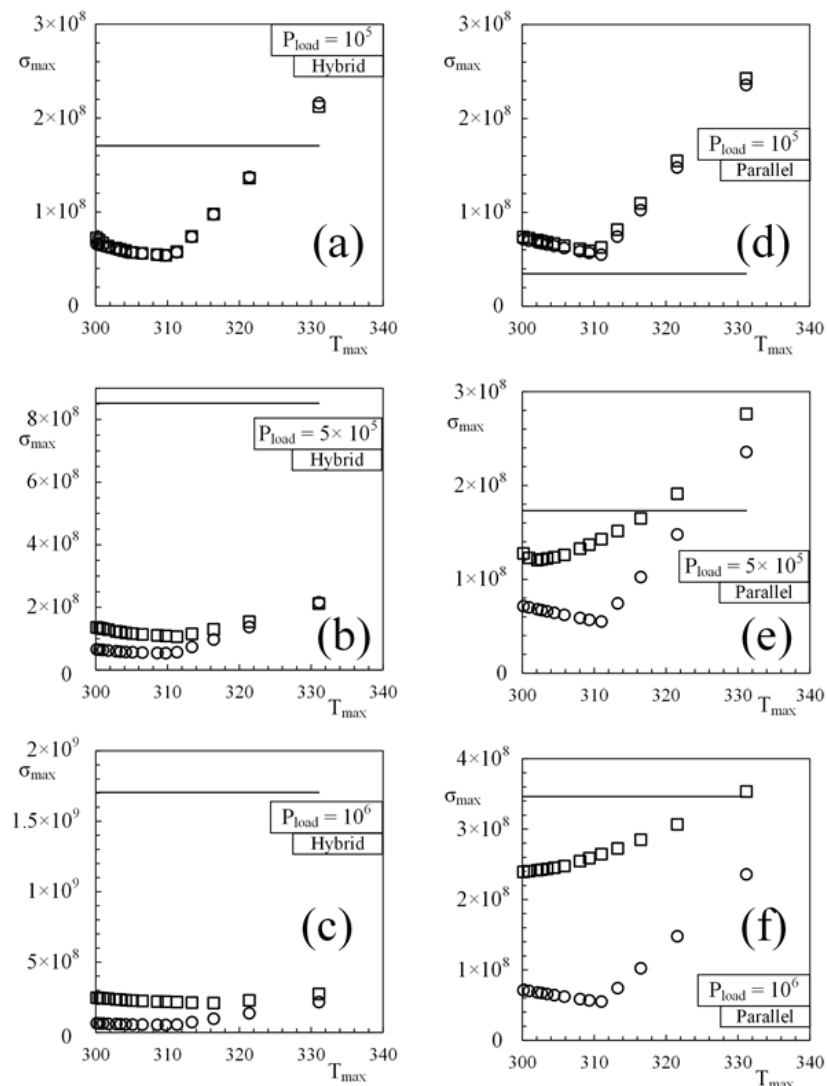
Figure 5. The effect of the maximum temperature on the peak stress for sole mechanical and thermal stresses and the coupled stresses with hybrid design when the load is (a) 10^5, (b) 5×10^5 and (c) 10^6 and with semi-circular design when (d) 10^5, (e) 5×10^5 and (f) 10^6

THE EFFECTS OF HEATING AND REFERENCE TEMPERATURE

Next, consider that the heating rate varies from 5 kW/m² to 2 and 10 kW/m². Figure 6a and b show how the peak stress varies relative to the maximum temperature for circular hybrid and semi-circular parallel channels when the heating rate is 2 and 10 kW/m², respectively. Both figures show that the peak stress decreases as the maximum temperature increases from 297 K to 310 K, and it is the minimum at 310 K. Then, increasing the maximum temperature increases the peak stress when the mechanical load is fixed at 10^5 Pa. Figure 6a shows that as the maximum temperature increases from 310 K to 360 K, the peak stress increases more than five times. However, it should be remembered that the effect of thermal stresses dominates the stress field when the mechanical load is 10^5 as shown in Figure 5. In addition, Figures 6a and b show that the peak stress varies in between 2-10% for the same maximum temperature value. This difference is expected because the thermal stresses is the function of temperature distribution in the entire domain. Varying the heating rate changes the temperature distribution even for the same maximum temperature cases.

Figures 7a and b show how the peak stress varies relative to the maximum temperature for circular hybrid and semi-circular parallel designs for variable reference temperature: 283, 303 and 323 K. The relation between the peak stress and the maximum temperature is the same for parallel and hybrid designs. The peak stress increases as the peak temperature increases when the reference temperature is 283 K.
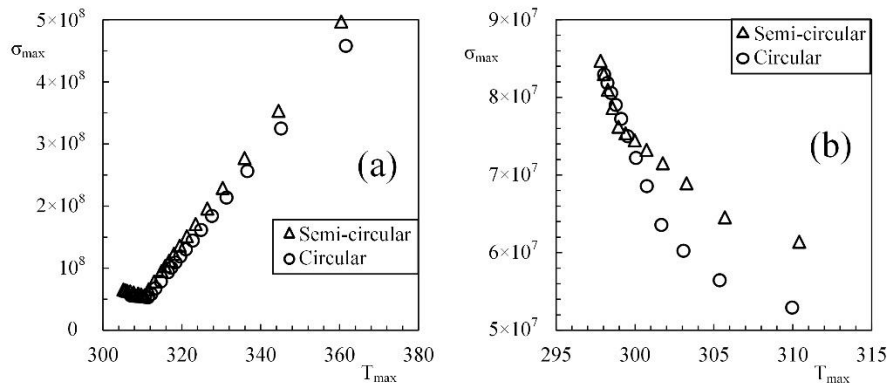
Figure 6. The peak stress relative to the maximum temperature with heating rate of (a) 10 and (b) 2 kW/ m^2 for hybrid and parallel designs

The peak stress decreases as the peak temperature increases from 304 K to 310 K, and then it increases as the temperature increases when the reference temperature is 303 K. Last, the peak stress decreases as the peak temperature increases when the reference temperature is 323 K. These results show that the peak stress becomes the minimum when the peak temperature is slightly greater than the reference temperature (~7 K when the reference temperature is 303 K). Figure 6 also shows that the curves for the reference temperatures of 283 and 323 K behaves as the curve with the reference temperature of 303 K but only tendency before and after the minimum peak stress behaviours exist, respectively.
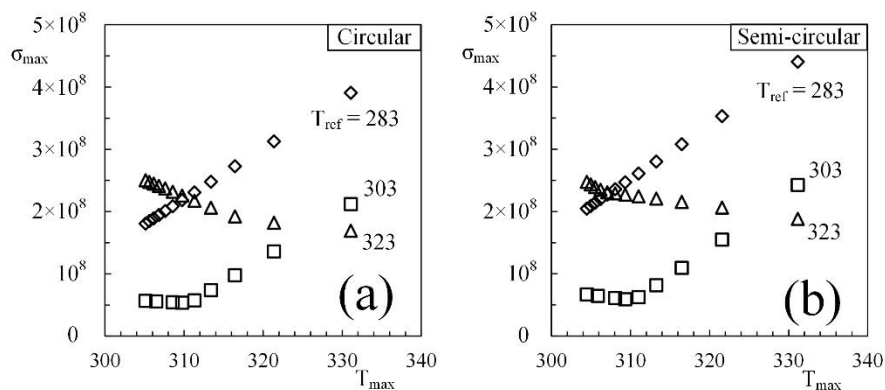

Figure 7. The peak stress relative to the maximum temperature with reference temperatures of 283, 303 and 323 K for (a) hybrid and (b) parallel designs

Figure 8 shows the temperature and von Mises stress distributions on the top surface (x-y plane of Figure 1) for the parallel and hybrid configurations when the pressure difference in between the inlet and outlet ports are 150 and 400 Pa. The temperature distributions show that the domain in between the inlet port and the distributing channels is relatively cold than the rest of the domain. In addition, they also show that the cold fluid is not uniformly distributed along the distributing channel, and therefore the temperature increases along the main distributing channel rapidly. In addition, the temperature contours show that the embedded channels provide better cooling as the pressure drop increases, i.e. domain near the distributing channels becomes relatively colder which makes visible the design of embedded cooling channels. Figure 8 also shows the distribution of von Mises stress for hybrid and parallel designs. These contours show that the peak stress occurs in between the main distributing and collecting channels and the corners of the plate. The order of the stress decreases as the pressure difference increases due to decrease in the temperature difference inside the plate. This decreases the stress related with the thermal expansion. The stress distributions are as expected because the positions of the corners are fixed and the mechanical load is applied perpendicular to the x-y plane. Therefore, the displacement along the z direction of the center in x-y plane is maximum, and the displacement is minimum near the corners.
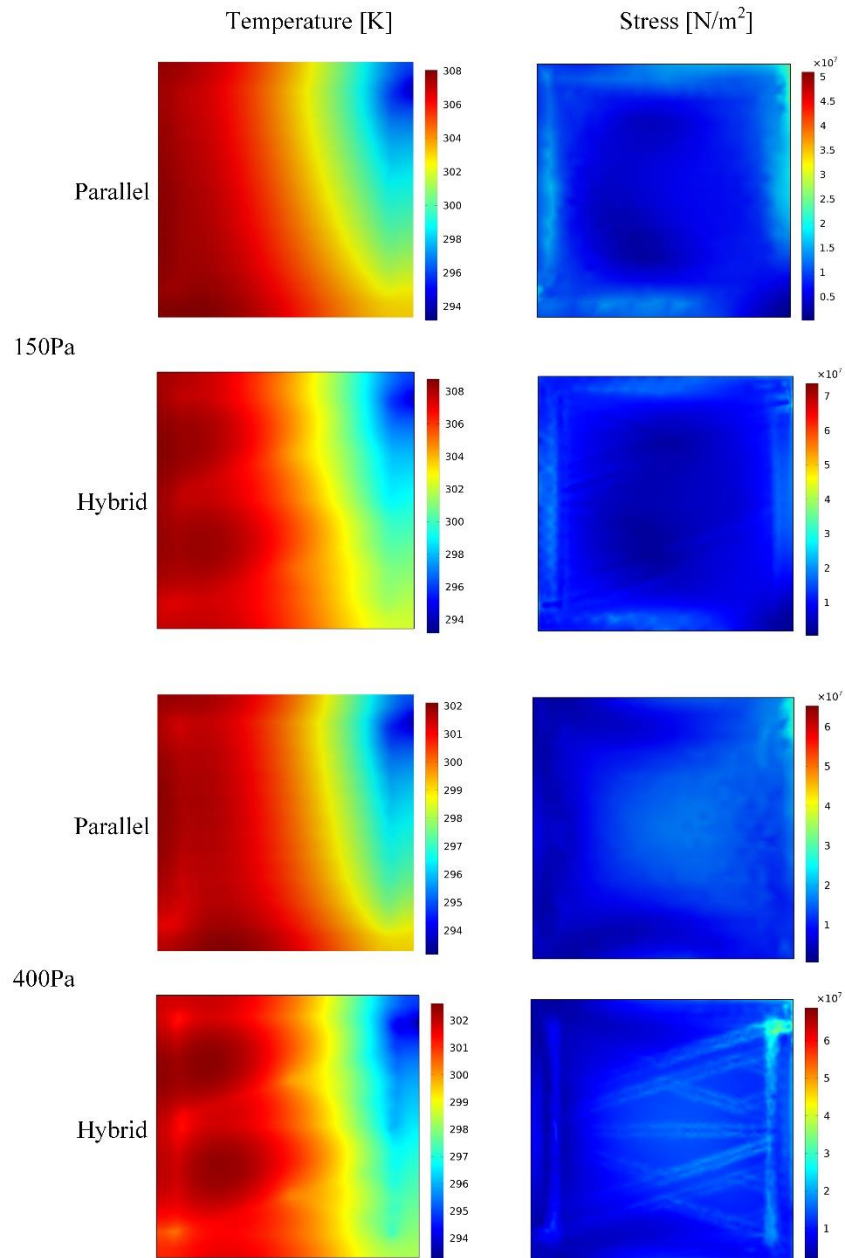
Figure 8. Temperature and von Misses stress distribution on the x-y plane for parallel and hybrid designs with 150 and 400 Pa pressure difference

CONCLUSION

This paper shows how the design should be morphed in order to decrease the resistances to the flows of fluid, heat and stresses. The designs corresponding to the smaller resistances for fluid, heat and stress flows vary for the discussed boundary conditions and assumptions. For instance, resistances to the fluid flow is smaller with circular hybrid channels than the parallel semi-circular channels. Whereas, thermal resistances are smaller with parallel semi-circular channel configuration (the peak temperature is 0.3% smaller than the circular hybrid configuration). These show that even one design corresponds to a smaller resistance to the flow of fluid that does not mean that is the best design when flow of heat and stress exist. In addition, the flow system should be considered as a coupled system as segregated solutions do not agree with the coupled solutions. In coupled solutions, all the governing equations were solved simultaneously, therefore, the effect of temperature on the material properties were uncovered in addition to the effect of deformation on the resistances to the heat and fluid flow.

In addition, this paper shows that thermal stresses may reduce the peak stress when they create additional resistance to the applied mechanical load. The thermal expansion creates an additional support for the mechanically loaded plate. The hybrid design with circular channels provides the smallest peak stress when the stress distribution consists of thermal stresses and mechanical stresses (due to the mechanical load). The maximum temperature corresponding to the minimum peak stress is also affected by the strain reference temperature. Overall, one should design the vascular structure based on the design needs and limitations.

In summary, the semi-circular channels provide smaller thermal resistance in comparison to the circular channels for the same flow volume in low flow rates. As the flow rate increases, the effect of design on the thermal performance diminishes due to the decrease in the conductive thermal resistances (i.e., the effect of conductive resistances becomes negligibly small). However, altering the design from semi-circular parallel to the circular hybrid promises smaller resistances to the flow of fluid and stresses and almost the same resistance to the flow of heat. This result uncovers that the morphing the design freely may uncover the design corresponding to the smallest resistance, and this design varies as the boundary conditions and assumptions vary. This is in accord with the constructal law, i.e. the freedom to morph promises to uncover the designs with better performance than the dictated designs.

NOMENCLATURE

c_p specific heat at constant pressure, $J\ kg^{-1}\ K^{-1}$
d   diameter of cooling channels, m
E   elasticity modulus, $N\ m^{-2}$
k   thermal conductivity, $W\ m^{-1}\ K^{-1}$
n   normal direction
P   pressure, $N\ m^{-2}$
P_{in} inlet pressure, $N\ m^{-2}$
q"   imposed heat flux, $W\ m^{-2}$
$r_{x,y,z}$ displacements, m
T   temperature, K
u, v, w velocity components, $m\ s^{-1}$
V   Volume, m^3
x, y, z coordinates, m
α thermal expansion coefficient, K^{-1}
γ Poisson ratio
ΔP Pressure difference $(P_{in} - P_{out})$, $N\ m^{-2}$
ε strain
μ dynamic viscosity, $kg\ m^{-1}\ s^{-1}$
ν kinematic viscosity, $m^2\ s^{-1}$
ρ density, $kg\ m^{-3}$
σ normal stress, $N\ m^{-2}$
τ shear stress, $N\ m^{-2}$
φ shear strain
0   main distributing channel
1   first level of cooling channel
2   second level of cooling channel
3   third level of cooling channel
f   fluid
in   inlet
m   mechanical
max   maximum
ref   reference
s   solid
out   outlet
x, y, z coordinates

REFERENCES

[1] Çetkin, E. (2015). Inverted fins for cooling of a non-uniformly heated domain. Journal of Thermal Engineering, 1(1), 1-9.

[2] Cetkin, E., & Oliani, A. (2015). The natural emergence of asymmetric tree-shaped pathways for cooling of a non-uniformly heated domain. Journal of Applied Physics, 118(2), 024902.

[3] Sakanova, A., Keian, C. C., & Zhao, J. (2015). Performance improvements of microchannel heat sink using wavy channel and nanofluids. International Journal of Heat and Mass Transfer, 89, 59–74.

[4] Minea, A. A. (2015). Numerical studies on heat transfer enhancement and synergy analysis on few metal oxide water based nanofluids. International Journal of Heat and Mass Transfer, 89, 1207–1215.

[5] Shafahi, M., Bianco, V., Vafai, K., & Manca, O. (2010). Thermal performance of flat-shaped heat pipes using nanofluids. International Journal of Heat and Mass Transfer, 53(7–8), 1438–1445.

[6] Li, Y., Xie, H., Yu, W., & Li, J. (2015). Liquid Cooling of Tractive Lithium Ion Batteries Pack with Nanofluids Coolant. Journal of Nanoscience and Nanotechnology, 15(4), 3206–3211.

[7] Alshaer, W. G., Nada, S. A., Rady, M. A., Del Barrio, E. P., & Sommier, A. (2015). Thermal management of electronic devices using carbon foam and PCM/nano-composite. International Journal of Thermal Sciences, 89, 79-86.

[8] Li, T., Lee, J.-H., Wang, R., & Kang, Y. T. (2014). Heat transfer characteristics of phase change nanocomposite materials for thermal energy storage application. International Journal of Heat and Mass Transfer, 75, 1–11.

[9] Ma, T., Yang, H., Zhang, Y., Lu, L., & Wang, X. (2015). Using phase change materials in photovoltaic systems for thermal regulation and electrical efficiency improvement: a review and outlook. Renewable and Sustainable Energy Reviews, 43, 1273-1284.

[10] Cetkin, E., Lorente, S., & Bejan, A. (2012). Vascularization for cooling a plate heated by a randomly moving source. Journal of Applied Physics, 112(8), 084906.

[11] Cetkin, E., Lorente, S., & Bejan, A. (2011). Vascularization for cooling and mechanical strength. International Journal of Heat and Mass Transfer, 54(13–14), 2774–2781.

[12] Wang, K. M., Lorente, S., & Bejan, A. (2009). The transient response of vascular composites cooled with grids and radial channels. International Journal of Heat and Mass Transfer, 52(19–20), 4175–4183.

[13] Rocha, L. A. O., Lorente, S., & Bejan, A. (2009). Tree-shaped vascular wall designs for localized intense cooling. International Journal of Heat and Mass Transfer, 52(19–20), 4535–4544.

[14] Cetkin, E., Lorente, S., & Bejan, A. (2011). Hybrid grid and tree structures for cooling and mechanical strength. Journal of Applied Physics, 110(6), 064910.

[15] Yenigun, O., & Cetkin, E. (2016). Experimental and numerical investigation of constructal vascular channels for self-cooling: Parallel channels, tree-shaped and hybrid designs. International Journal of Heat and Mass Transfer, 103, 1155–1165.

[16] Cho, K. H., Lee, J., Ahn, H. S., Bejan, A., & Kim, M. H. (2010). Fluid flow and heat transfer in vascularized cooling plates. International Journal of Heat and Mass Transfer, 53(19–20), 3607–3614.

[17] Cho, K. H., Chang, W. P., & Kim, M. H. (2011). A numerical and experimental study to evaluate performance of vascularized cooling plates. International Journal of Heat and Fluid Flow, 32(6), 1186–1198.

[18] White, S. R., Sottos, N. R., Geubelle, P. H., Moore, J. S., Kessler, M., Sriram, S. R., ... & Viswanathan, S. (2001). Autonomic healing of polymer composites. Nature, 409(6822), 794-797.

[19] Hamilton, A. R., Sottos, N. R., & White, S. R. (2010). Self-healing of internal damage in synthetic vascular materials. Advanced Materials, 22(45), 5159–5163.

[20] Bejan, A., Lorente, S., & Wang, K. M. (2006). Networks of channels for self-healing composite materials. Journal of Applied Physics, 100(3), 033528.

[21] Wang, K. M., Lorente, S., & Bejan, A. (2010). Vascular structures for volumetric cooling and mechanical strength. Journal of Applied Physics, 107(4), 044901.

[22] Çetkin, E. (2015). Constructal structures for self-cooling: microvascular wavy and straight channels. Journal of Thermal Engineering, 1(5), 166-174.

[23] Rocha, L. A. O., Lorente, S., & Bejan, A. (2014). Vascular design for reducing hot spots and stresses. Journal of Applied Physics, 115(17), 174904.

[24] Cetkin, E., Lorente, S., & Bejan, A. (2015). Vascularization for cooling and reduced thermal stresses. International Journal of Heat and Mass Transfer, 80, 858–864.

[25] Multiphysics, C. O. M. S. O. L. (2005). Comsol, Inc. Burlington, MA.